34th Space Symposium, Technical Track, Colorado Springs, Colorado, United States of America
Presented on April 16, 2018

METHODOLOGY AND RESULTS OF JAMES WEBB SPACE TELESCOPE THERMAL VACUUM OPTICAL SYSTEM ALIGNMENT TESTING AND ANALYSIS

Koby Z. Smith
Ball Aerospace, ksmith@ball.com

D. Scott Acton, Laura E. Coyle, Taylor S. Chonis, Ben Gallagher, J. Scott Knight
Ball Aerospace, dsacton@ball.com, lecoyle@ball.com, tchonis@ball.com, jsknight@ball.com

ABSTRACT

The James Webb Space Telescope (JWST) project is an international collaboration led by NASA's Goddard Space Flight Center (GSFC) in Greenbelt, MD. The Webb Telescope is NASA's flagship observatory that will operate nearly a million miles away from Earth at the second Lagrange point. Webb's optical design is a three-mirror anastigmat with four main optical systems; 1) the eighteen active Primary Mirror Segment Assemblies (PMSA), 2) a single active Secondary Mirror Assembly (SMA), 3) an Aft-Optics Subsystem (AOS) consisting of a Tertiary Mirror and Fine Steering Mirror, and 4) an Integrated Science Instrument Module (ISIM) consisting of the various instruments for the Webb Telescope. Webb's optical system has been designed to accommodate a significant amount of alignment capability and risk with the PMSAs and SMA having rigid body motion available on-orbit for alignment to the essentially fixed AOS and ISIM optical systems.

Two critical pieces of information for the ground-test of such a large, segmented, active telescope is to 1) ensure that the relative alignment of the fixed optical sub-systems (AOS & ISIM) meet expectations, and that 2) the active components of the system (PMSAs & SMA) have adequate range of motion to align to the fixed optical subsystems once on-orbit. Addressing these two critical system parameters, a novel approach utilizing single-image phase retrieval of highly aberrated ground-test images combined with spatial metrology was developed to assess the relative alignment of the fixed optical sub-systems, and an innovative sparse-aperture test technique combining the classical optical Hartmann test with the active primary mirror segments was developed to assess the relative optical alignment of the PMSAs and SMA to the AOS & ISIM. This paper presents the methodology and results of these approaches implemented on the James Webb Space Telescope during cryogenic thermal vacuum testing at Johnson Space Center in Houston, TX..

1.0 JAMES WEBB SPACE TELESCOPE ARCHITECTURE OVERVIEW

The Webb Telescope is an infrared, cryogenic astronomical observatory that will operate in an orbit about the second Lagrange point. Webb has a large 6.5m diameter primary mirror and a suite of infrared instruments that are necessary to meet the science mission's sensitivity requirements. The importance and goals of the mission have required a number of different instruments to operate onboard Webb; near- and mid-infrared imagers, near- and mid-infrared spectrometers, and guiders. The relatively large quantity of instruments performing near-simultaneous imaging required a large, well-corrected field of view, which led the optical design of Webb to a three-mirror anastigmat[1]. The three-mirror anastigmat is a modified form of a classical Cassegrain telescope where there is a nearly parabolic primary mirror, a convex hyperbolic secondary, and a concave elliptical tertiary mirror. The Webb telescope's design also incorporates a fine steering mirror to both fold the optical system and provide fine image stabilization.

The implementation of this design for a space-based observatory requires it to fit within the fairing of an Ariane 5 launch vehicle, which in turn requires the telescope to be folded and stowed (Figure 1). The sides of the primary mirror are folded and the secondary mirror and its support structure are folded as well. The need to fold and stow the telescope as well as manage the uncertainty in the deployment and operation of a cryogenic

telescope nearly a million miles away from the Earth required an active telescope system architecture to accommodate on-orbit alignment risk[1,2].

The Webb Telescope's four primary optical systems accommodate that type of architecture (Figure 2); 1) the eighteen active Primary Mirror Segment Assemblies (PMSA), 2) a single active Secondary Mirror Assembly (SMA), 3) an Aft-Optics Subsystem (AOS) consisting of a Tertiary Mirror and Fine Steering Mirror, and 4) an Integrated Science Instrument Module (ISIM) consisting of the various instruments for the Webb Telescope.

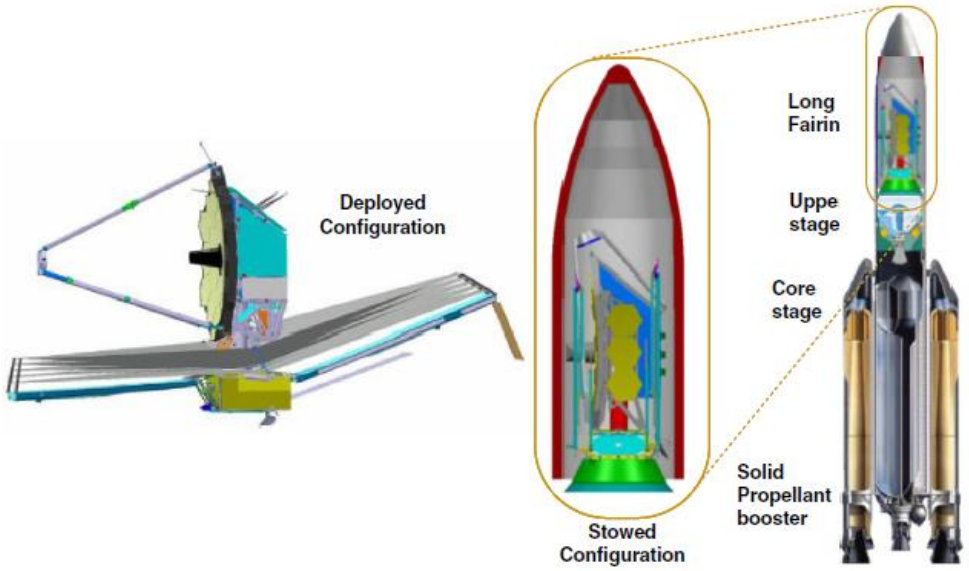

Figure 1. The deployed configuration of the Webb Telescope (left) and the Webb Telescope stowed in the fairing of the Ariane 5 (right)[1].

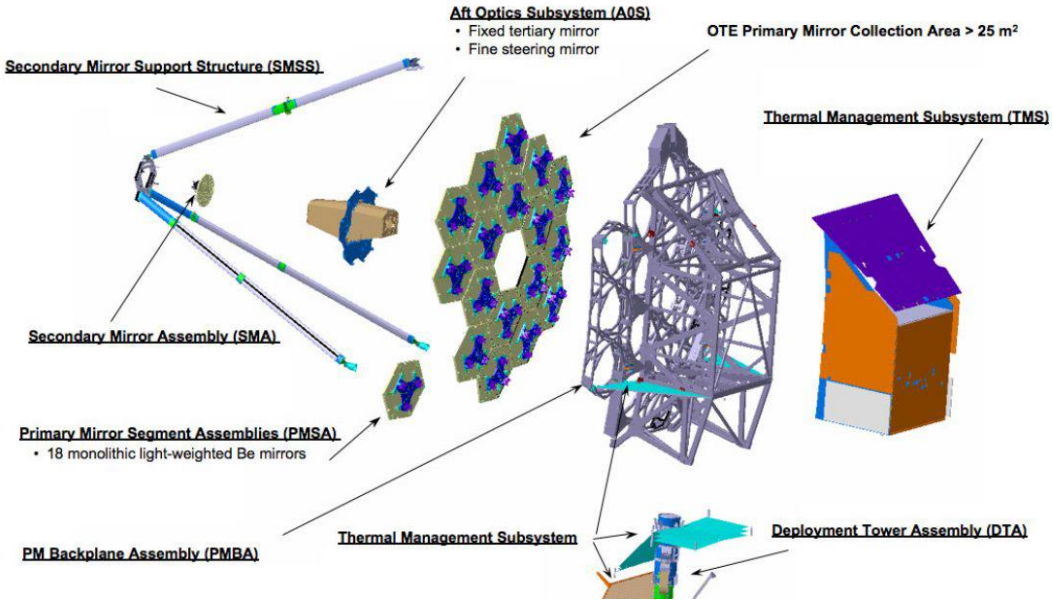

Figure 2. Exploded view of the Webb Telescope's primary systems.

The primary mirror is composed of quantity 18 light-weighted beryllium mirror segment assemblies that utilize a semi-rigid mirror archietecture[1]. The primary mirror segment assemblies (PMSA) consist of the light-weighted

mirror itself, a cryogenic hexapod system that provides six degrees-of-freedom adjustment, and a radius of curvature actuator that allows each segment's radius to be adjusted. This semi-rigid mirror architecture allows the segmented primary mirror to adjust to a relatively large amount of prescription and wavefront aberration forms to accommodate a significant amount of alignment and optical performance risk.

The secondary mirror assembly (SMA) has a rigid-mirror architecture that consists of a light-weighted beryllium mirror with a cryogenic hexapod system that provides six degrees-of-freedom adjustment. There is no radius of curvature adjustment on the secondary mirror. The adjustment of the secondary mirror is a primary lever in the overall alignment of the telescope on-orbit.

The aft-optics subsystem (AOS) consists of the light-weighted tertiary mirror assembly (TMA) and the fine steering mirror (FSM) in a beryllium bench. The alignment of the AOS components are fixed and as such are considered the optical alignment reference for the telescope[3], meaning that the primary mirror and secondary mirror are aligned to the AOS. The FSM has the capability to tilt to support image stabilization.

The integrated science instrument module (ISIM) is a composite bench containing quantity seven unique science instruments. The instruments are all rigidly mounted to the composite bench, but 6 of the 7 instruments have a relatively small focus adjustment mechanism to accommodate subtle focus variation over the field of view or individual instrument focus variation.

This type of optical system architecture is a very pragmatic approach to large, deployable, space telescope systems that are not serviceable by providing active alignment capability on-orbit. However, the system has finite alignment capability and therefore ground-based integration and test efforts should focus on 1) verifying the relative alignment of the fixed optical subsystems and 2) verifying that the active optical subsystems are aligned to their expected ground-test locations and will have adequate range to accommodate the risks in the overall system[2]. This paper will discuss the cryogenic test program that was implemented on the Webb Telescope's optical systems to verify those very things.

2.0 JAMES WEBB SPACE TELESCOPE CRYOGENIC TEST OVERVIEW

Prior to launch, the Webb Telescope Optical Telescope Element (OTE) and Integrated Science Instrument Module (ISIM), which when assembled together are identified by the acronym OTIS, underwent various environmental test programs. One of these environmental test programs was the cryogenic thermal vacuum testing that occurred in the Johnson Space Center (JSC) Chamber "A" facility in Houston, TX[4]. Included within the Chamber A cryogenic testing program were two optical test sub-programs; the first optical test sub-program was called Pathfinder and utilized a subset of flight-like test hardware and actual OTIS test hardware for the purposes of risk reduction[5], and the second optical test sub-program is the actual cryogenic testing of the flight OTIS hardware itself (see Figure 3).

The ground-testing of a large, deployable, space telescope is a significant and costly endeavor, especially if the desire is to have a full-aperture end-to-end performance test. The development of equipment and hardware to support such a test can be as expensive and complex as some of the telescope elements under test. Therefore, a different approach to the final cryogenic ground test was taken with the Webb telescope. The individual Webb optical components and assemblies' performance had been thoroughly verified at cryogenic temperatures prior to integration to the telescope assembly. This allowed the primary goal of the final OTIS cryogenic vacuum testing to verify the alignment of the system on the ground to ensure that alignment could be achieved on-orbit. In brief summary, the purpose of the JSC OTIS testing[6] is to 1) verify the relative optical alignment of the Aft-Optics Subsystem (AOS) to the ISIM, 2) demonstrate that the quantity 18 primary mirror segment assemblies (PMSA) can be aligned and phased into a single global primary mirror within expectations due to ground test, 3) verify expected ground-test alignment of the PMSAs and Secondary Mirror Assembly (SMA) to the AOS, 4) cross-check the measured wavefront of the AOS itself and the OTE as a whole, and 5) demonstrate a subset of various flight-like wavefront sensing and control operations.

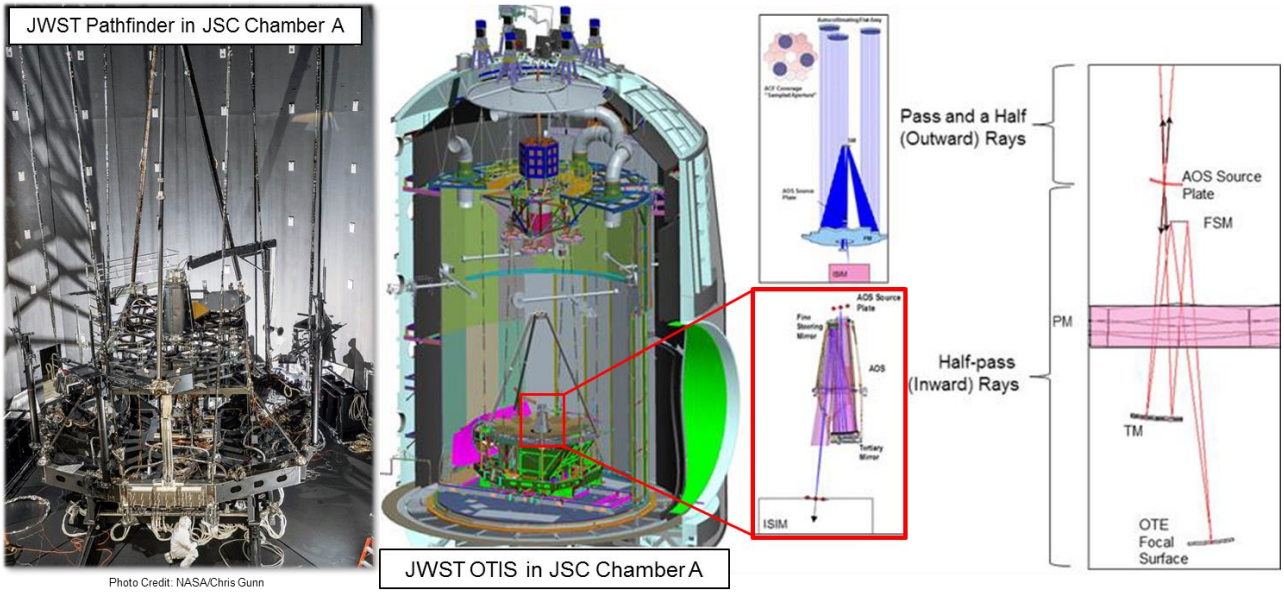

Figure 3. JWST Pathfinder and OTIS Test Layouts within JSC Chamber A.

The scope of this paper is primarily concerned with #1 and #3 listed above, which is to verify the relative optical alignment of the AOS to ISIM and cross-check the expected ground-test alignment of the PMSAs and Secondary Mirror Assembly (SMA) to the AOS. The AOS and ISIM are essentially the only fixed optical subsystems within JWST, and therefore the cryogenic alignment of the AOS to the ISIM is critical to the optical performance and mission success of JWST. The cross-check of the ground-test alignment of the PMSAs and the SMA is vital to ensure that there will be sufficient actuator range on-orbit to accommodate risks.

2.1 Methodology for the Cryogenic Alignment Assessment of Aft-Optics Subsystem (AOS) to the Integrated Science Instrument Module (ISIM)

With the active control systems on the PMSA and SMA segments, the cryogenic optical alignment of the AOS to ISIM is the anchor to the JWST optical system. Significant thought and planning went into the methodology and approach that was used to quantify this AOS to ISIM alignment[7,8]. The three-mirror anastigmat optical design of JWST has an intermediate focus between the SMA and tertiary mirror (TM) of the AOS (essentially the Cassegrain focus of the PM/SM combo), and this intermediate focus allowed for an opportunity with regard to the optical testing of the system. Optical sources placed at the intermediate focus can be imaged by the AOS onto the OTE focal surface, which are then collected by ISIM. This is known as the "inward" or "Half-Pass" test configuration (see Figure 4), since it only passes through half of the OTE elements (tertiary mirror and fine steering mirror). For reference, an additional set of optical sources located at the intermediate focus point "outward" for use in what is referred to as the "Pass-and-a-Half" test, which is covered in the next section. The inward or Half-Pass (HP) light path allows the AOS and ISIM optical performance to be interrogated by themselves, without any influence from the primary mirror, secondary mirror, or auto-collimating flats.

Since the intermediate focus of JWST is located very close to an AOS bulkhead, those inward optical sources can be physically attached to the AOS during ground testing. Therefore, if the wavefront and location of the inward source images produced by the AOS near and around the OTE focal surface are characterized with respect to the AOS datums, then any inward source image collected near the OTE focal surface can provide information on its relative location to the AOS datum. In this manner the AOS can provide an optical yardstick by which the instruments within ISIM can evaluate their relative positions to and the alignment of the AOS to ISIM can be

quantified. This approach led to the design and development of the AOS Source Plate Assembly (ASPA) and the test methodologies that go along with it[9]. ASPA is a chassis that attaches to the FSM bulkhead of the AOS and contains fiber optic sources used for Half-Pass and Pass-and-a-Half testing in OTIS (see Figure 5). Detailed information on ASPA can be found in the reference material[8].

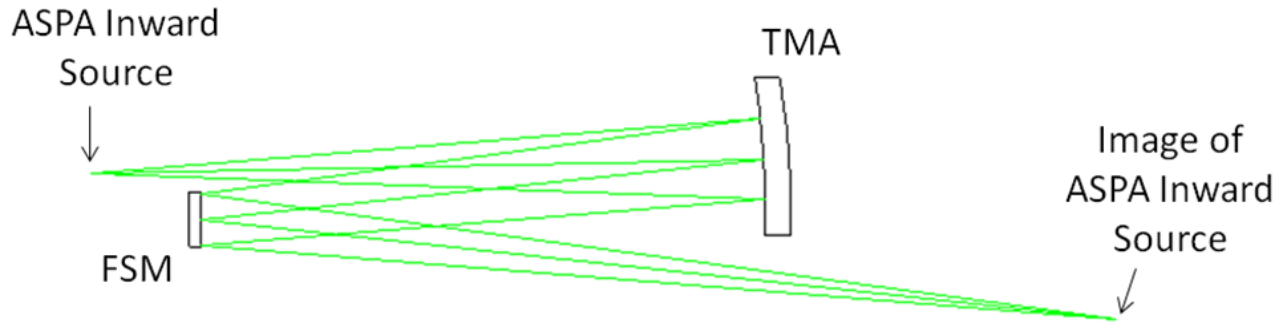

Figure 4. Inward or "Half-Pass" optical test layout of the AOS. The Fine Steering Mirror (FSM) and Tertiary Mirror Assembly (TMA) make up the AOS.

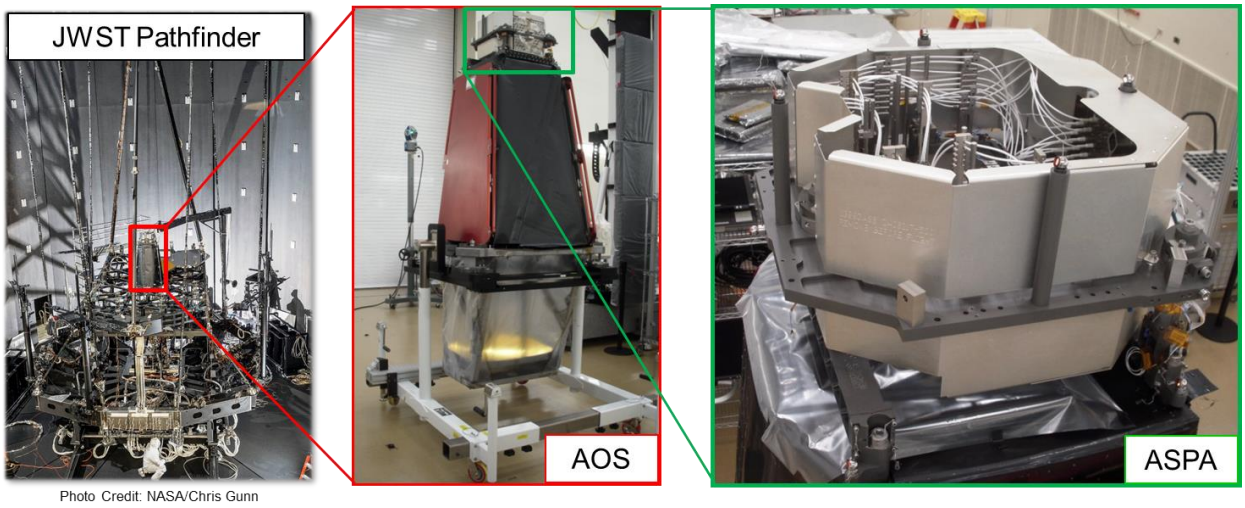

Figure 5. The ASPA chassis as installed on the AOS and in the JWST Pathfinder assembly.

There are quantity seven locations within the JWST field of view that are sampled by different science instruments within ISIM and they are: 1) NIRCam A, 2) NIRCam B, 3) FGS1, 4) FGS2, 5) NIRISS, 6) NIRSpec, and 7) MIRI. Inward sources are located within ASPA to produce inward source images in each of these instruments' fields of view. In this manner, examining the images for both location (on the detector) and the amount of wavefront focus at each instrument location across the field of view can be used to determine AOS to ISIM axial, lateral, tilt (also measured via pupil alignment), and clocking alignment[7]. Figure 6 provides a map of the science instruments' field of view footprints on the OTE focal surface along with the locations where ASPA inward source images are expected to be.

Inherent to the optical design of the three-mirror anastigmat is that the three aspheric mirrors are used off-axis in field in order to provide compensating wavefront effects to produce diffraction-limited imagery at the final image surface over a relatively large field of view[10]. A non-subtle nuance to the half-pass test is the fact that the AOS (actually just the tertiary mirror) is only one-third of the three-mirror anastigmat and with the inward sources at the intermediate focus of JWST, the elliptical tertiary mirror is still being used off-axis in field and does not have the compensating effects of the secondary mirror and primary mirror to balance the wavefront quality. As such,

the inward source images have approximately 2 - 3µm RMS of wavefront error, primarily 3rd order coma and astigmatism, depending on the field location. An example of the modeled point spread function (PSF) of the inward source image at NIRCamB (one of the closest to on-axis of JWST) at various thru-focus positions in shown in Figure 7. These images show the severe amount of coma and astigmatism that is present.

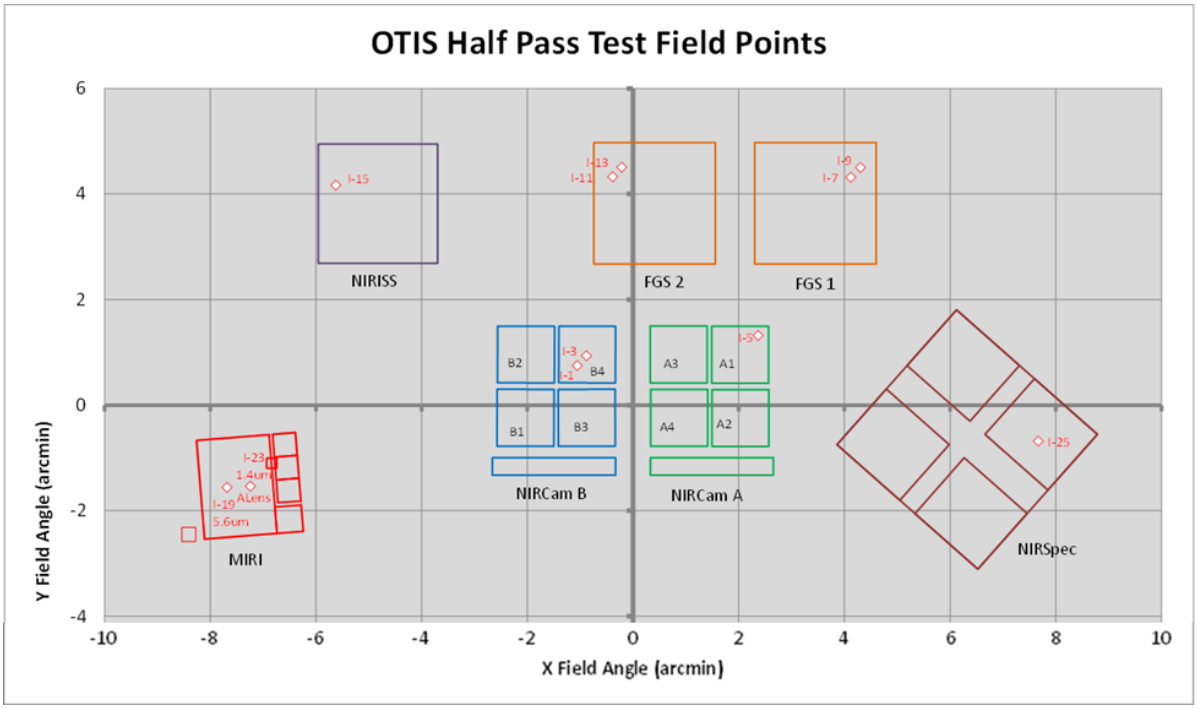

Figure 6. Webb Telescope field of view along with science instrument footprints and ground-test field locations (diamonds).

Given the structure, the density of the fringes, and intensity variation in the inward source image PSFs, traditional image alignment techniques utilizing various centroiding techniques and encircled energy analyses will not provide sufficiently accurate image position and wavefront focus information respectively. After an initial analysis, it was decided that image-based phase retrieval would be used to quantify both image location and wavefront focus for a given image. While the core of the JWST wavefront sensing and control system utilizes advanced phase retrieval algorithms and techniques[11], phase retrieval on images with this level of wavefront error had not been documented in industry or academia before.

In combination with the phase retrieval analysis itself, spatial metrology techniques and tools utilizing laser trackers, laser radars, and photogrammetry systems were used to measure the location of the phase retrieval camera in order to connect the image and wavefront data to a physical location with respect to the AOS. All of the data in aggregate was used to create the calibration necessary for the AOS to ISIM alignment assessment[8]. The resulting calibration data product was a four-dimensional vector where the first three elements were the Cartesian coordinate of the image in a coordinate system defined by the AOS (e.g. XYZ), and the fourth element was the measured focus/power in the wavefront at that corresponding image location ([X,Y,Z,Z4]). In this manner the calibration vector provides both boresight and focus information that is used to correlate an optical model to determine the predictions for the OTIS cryogenic test. Figure 8 provides a map of the measured “best focus” Half-Pass images at each instrument over the Webb field of view.

Predictions for the expected image location and wavefront content for each instrument were created along with the predicted pupil alignment between the FSM aperture and the NIRCamB pupil. The actual measured

performance at each science instrument was then collected during the OTIS cryogenic testing and the errors to the predicts quantified. The data across the field of view is examined with a set of linear equations to solve the amount of rigid body alignment error the ISIM had with respect to the AOS, along with individual residual science instrument focus errors (Figure 9).

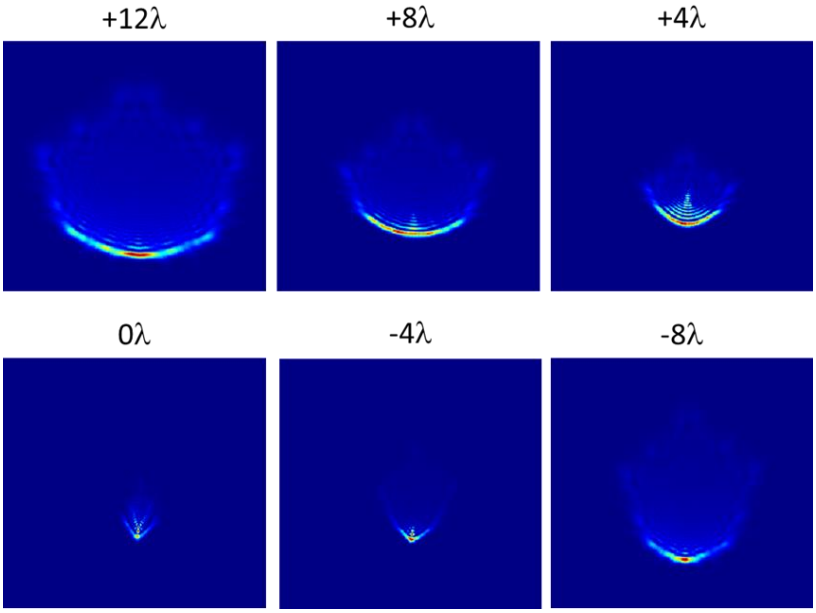

Figure 7. Modeled thru-focus point spread functions of ASPA inward source images at NIRCamB. The amount of defocus from "best focus" is expressed in peak to valley waves at 2120nm.

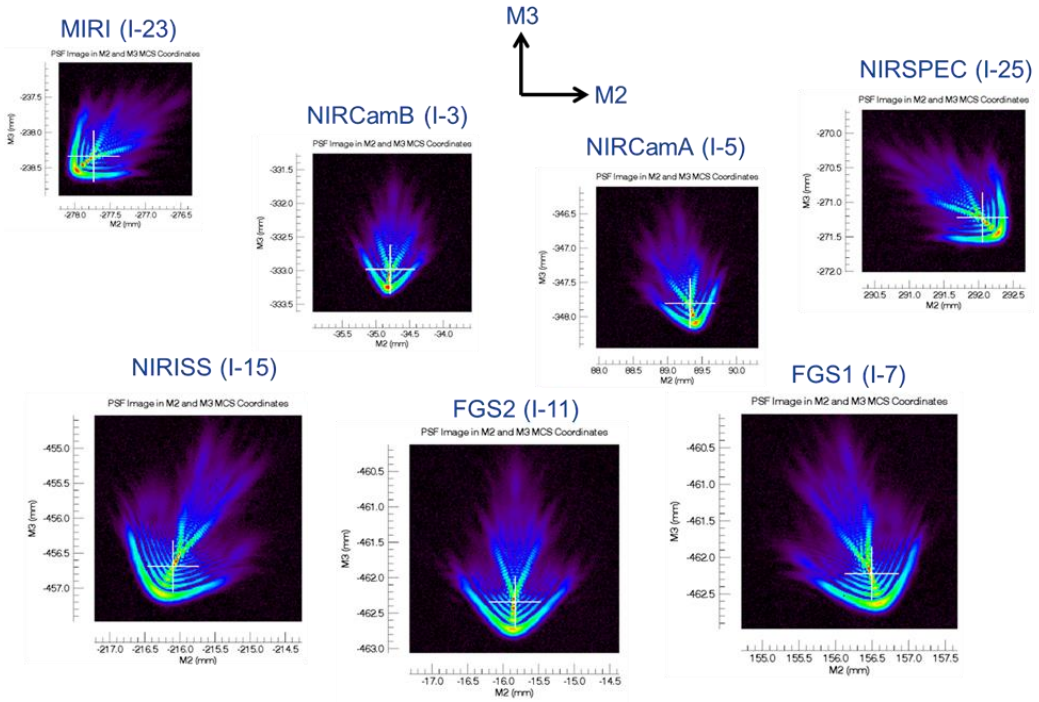

Figure 8. Point spread functions at best focus (Zernike power = 0nm) of various inward sources for each instrument over the OTE field of view. The point spread functions are identified by their ASPA ID# and are shown on scaled plots. The white cross-hairs in the images denote the zero-tilt location of the images, which is a phase-retrieval feature used to locate the images.

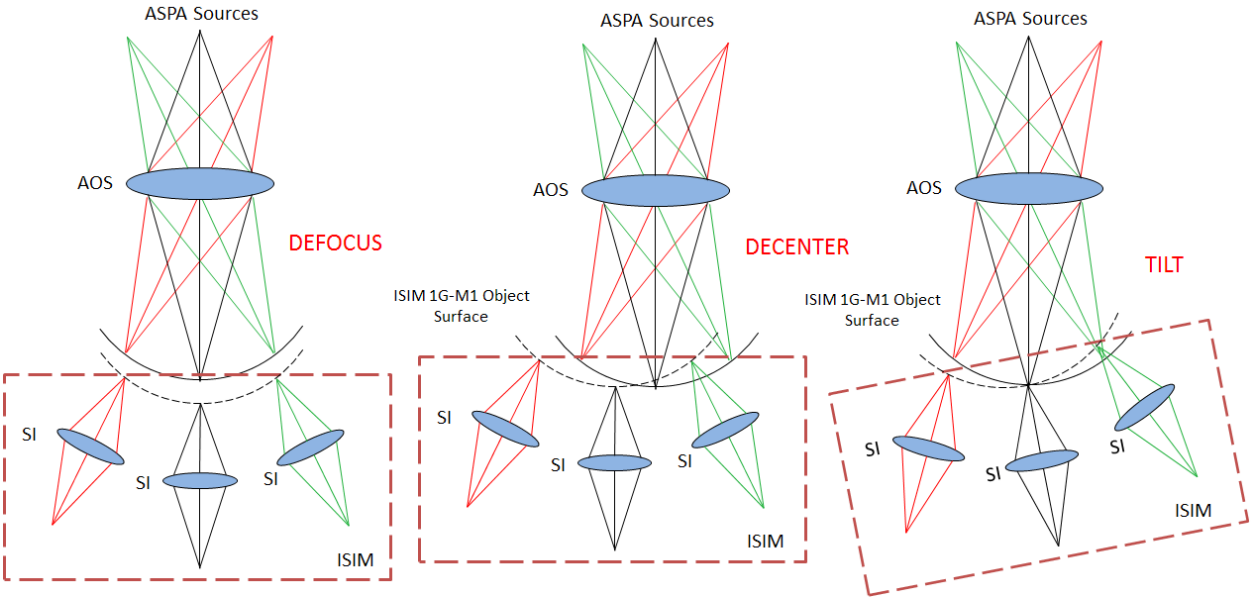

Figure 9. Simplistic examples of rigid body misalignments between AOS and ISIM.

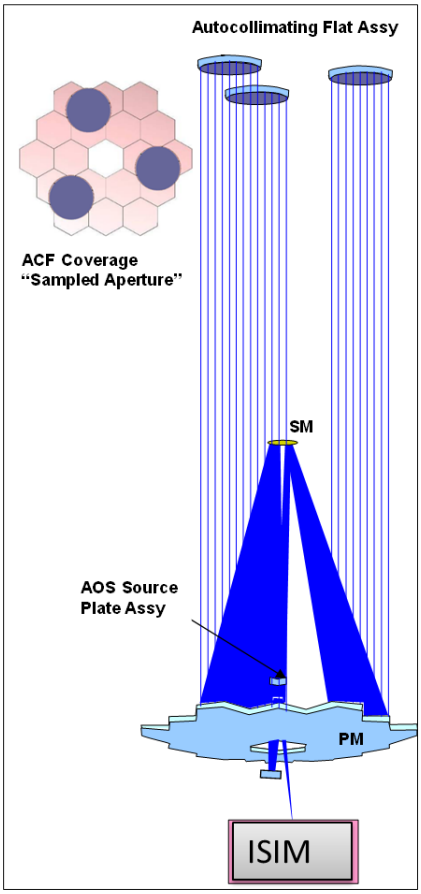

Figure 10. The layout of the "Pass-and-a-Half" (PAAH) test during the OTIS cryogenic test campaign.

2.2 Methodology to Crosscheck the Alignment of the Primary Mirror & Secondary Mirror to the Aft-Optics Subsystem

The cross-check of the primary mirror and secondary mirror alignment was a far more complex process as it required a number of other test activities to be completed prior to its execution, which won't be discussed in detail here. In summary though, the primary mirror segments were aligned to the AOS using a combination of photogrammetry[12] and a center-of-curvature interferometer[13]. Fiducials mounted to the edges of the mirror segments were used to place those particular segments to a defined ground test location based on their previously measured cryogenic performance. The center-of-curvature interferometer was then used to phase all eighteen primary mirror segments into an effective monolithic primary mirror. Similarly, the secondary mirror was aligned to a ground-test target position using photogrammetry. As such, both the primary mirror and the secondary mirror were aligned to the AOS using photogrammetry.

The "Pass-and-a-Half" (PAAH) test was used to assess the entire OTIS optical system path and provide a cross-check of the alignment of the primary mirror and secondary mirror using image data collected in the science instruments. As mentioned previously, the ASPA had a set of optical sources that faced "outward" or towards the secondary mirror. With ASPA located at the Cassegrain focus of the OTE, the light from the outward sources was collimated by the secondary mirror and primary mirror. That collimated light was then incident upon quantity three 1.5m diameter optical flats, known as auto-collimating flats (ACF), see Figure 10 and Figure 11.

Due to the cost and complexity of this cryogenic test, the quantity three ACF's were used in a sparse-aperture test format vs implementing a 6.5m diameter auto-collimating optic[4]. While not a full-aperture test, the sparse-aperture approach provides sufficient sensitivity to provide the crosscheck of the primary mirror and secondary mirror alignment and functionally test the entire OTIS optical path. Figure 11 highlights the relative size and alignment of the ACFs to the PMSA's. A single ACF diameter is equivalent to a PMSA diameter and positioned such that a single ACF covers three adjacent PMSAs of varying off-axis prescription (A, B, and C).

The ACFs were then tilted together to steer the collimated light back into the OTE at field angles that would direct the light to be incident upon each science instrument. This approach allowed the OTIS performance to be tested over the entire field of view, albeit in a sparse-aperture manner.

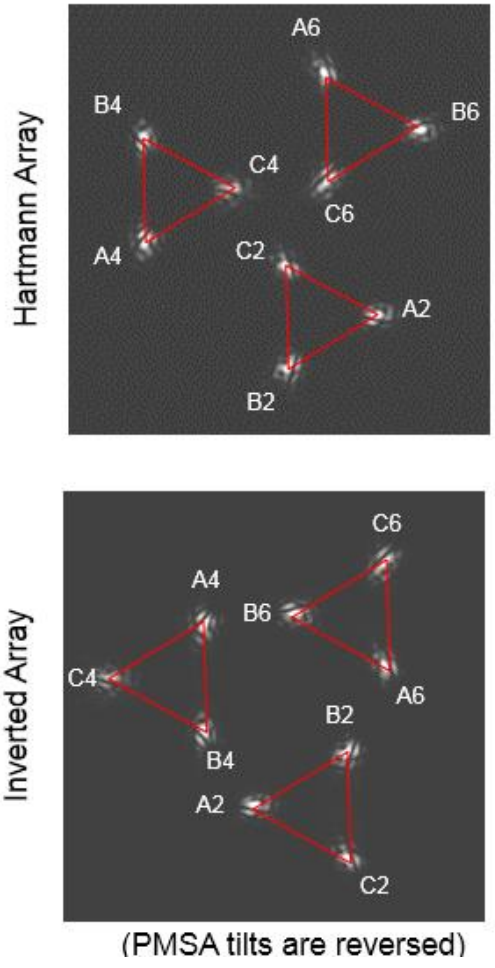

Figure 12. PAAH point spread function arrangements in the Hartmann Array and Inverted Hartmann Array.

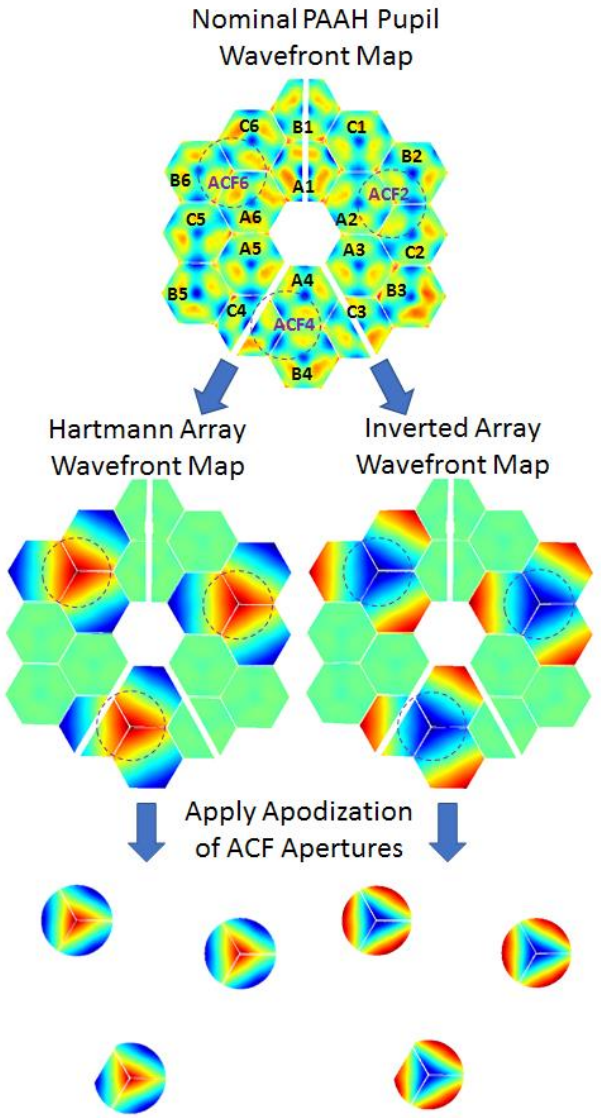

Figure 11. Spatial alignment of the three auto-collimating flats (purple dashed circles) with the primary mirror segments in the nominal ground-test PMSA wavefront map. Also showing the tilt induced on the nine PMSA segments to produce the Hartmann and Inverted Array. The final wavefront map is the sparse-aperture PAAH pupil for the two Hartmann array configurations.

Since the quantity three ACFs could not be phased in test, the baseline test approach was to effectively treat each image created by an ACF as a separate telescope and separate them on the instruments'

detectors. This would have created three unique images (one for each ACF) and phase retrieval would have been used to estimate the wavefront over each ACF sparse aperture. However, during the Pathfinder testing program, the level of vibration in the test was shown to be higher than what was allowable for the baselined PAAH phased primary mirror phase-retrieval test approach. An alternative test approach was developed based on the Hartmann test[14].

The baseline test approach would have produced wavefront maps over each ACF pupil that would then be used to estimate the wavefront error over the entire OTIS pupil. If one samples focus or third-order aberration (e.g., astigmatism, coma) over the OTIS pupil with the sparse-aperture test and then examines the wavefront over each of the pie-shaped PMSAs within each of the ACF pupils, the first and largest wavefront error term over a pie-shaped PMSA segment would be tilt. This is not surprising since it would be expected that the smaller aperture PMSAs are sampling a local slope within the larger global aberration over the OTIS pupil. This local sampling of slope over a global pupil function is exactly what the Hartmann test does.

With this concept in mind, a relatively simple modification to the baseline test approach was implemented. Instead of having a phased primary mirror over each ACF, each PMSA under an ACF would be tilted a small amount to allow each PMSA PSF to be easily identified on the detector. Each of the ACFs would then also be tilted to ensure that each group of three spots were sufficiently separated. This approach would produce nine unique PSFs on the science instruments, one PSF for each PMSA (see Figure 12). The PMSAs were tilted such that corner of each PMSA within a triad (the three PMSAs within an ACF) was high at the center of the ACF (Figure 11), which produced radial separation of the PSFs. This arrangement was known as the Hartmann Array. The alternative tilt direction of the PMSAs was also used, where the corner of each PMSA within a triad was low in the center of the ACF, and that arrangement was known as the Inverted Array. The combination of these array configurations ultimately allowed effects like plate scale errors or uncertainties to be averaged out.

For the sake of an example, one could imagine that if the primary mirror (global) and secondary mirror were aligned to nominal, then the PSF array formed by tilting each PMSA a known amount would produce a symmetrical array and any deviations to the symmetrical array would be due to wavefront aberrations in the pupil. Those PSF centroid deviations from the nominal array could be quantified and the resulting tilt over a PAAH PMSA calculated along with the best-fit wavefront to the those measured wavefront tilts. Alternatively, a system of linear equations could be built that represent the PSF centroid impacts due to various primary mirror and secondary mirror perturbations. The set of linear equations could be solved for the best-fit primary mirror or secondary mirror motion that fit the measured PSF centroid deviations. The sensitivity of this approach is documented in the reference material[14].

In the actual PAAH test, the optical model was used to generate the PSF target values for the Hartmann and Inverted Arrays in each science instrument. The metric used for this analysis were the individual leg lengths for each triad (e.g. A4 to B4, A4 to C4, and B4 to C4, red lines in Figure 12). The optical model target PSF centroid values were used to create target leg length values and the measured data was treated the same. The set of linear equations was then solved for the least squares solution to determine the secondary mirror focus along with secondary mirror tilt/decenter or primary mirror tilt that fit the measured leg length errors.

All of the data discussed to this point was collected using a single ASPA source and having the ACFs steer the light into each science instrument in a serial, timewise fashion (one at a time). In a special test configuration, which was called the Chandelier test, a set of three sources specifically positioned such that a single ACF tilt position would allow the light emitted from each of the three sources to land in three different science instruments at the same time (NIRCamA, FGS1, and NIRSS). This special test configuration allowed the test to become an all-relative test to NIRCamA for FGS1 and NIRISS. Since the data was collected at the exact same time in three different field points and is relative to NIRCamA, a number of error sources in the test are forgiven or reduced, such that the ability to detect variations in the pupil aberrations over the field was increased. This was particularly useful in detecting focus variation over the field.

One item to note is that the wavefront impact, and impact to the Hartmann arrays, from secondary mirror decenter, secondary mirror tilt, and primary mirror tilt are effectively identical as they all produce coma in the wavefront. Therefore, this optical crosscheck can't distinguish between these factors, it can only solve for how much of each factor could be causing the observed error. For the purposes of the cross-check to photogrammetry, this is completely adequate.

3.0 AFT-OPTICS SUSBSYSTEM (AOS) TO INTEGRATED SCIENCE INSTRUMENT MODULE (ISIM) CRYOGENIC ALIGNMENT RESULTS

The Half-Pass data across the field of view has been collected, processed, and independently verified to acceptable tolerances. An example of the data collected and processed is shown for an image in NIRCamA (Figure 14 & Figure 13). Once the image data was collected, the wavefront phase map and image location for each image were determined by the Phase Retrieval Metrology Software (PRMS) developed by Goddard Space Flight Center (GSFC). The phase retrieval results are used to create a three-element vector that represents the image location (X_{pixel}, Y_{pixel}) on the science instrument sensor chip assembly (SCA) and the amount of measured power (Z4) in the retrieved wavefront, [X_{pixel}, Y_{pixel}, Z4].

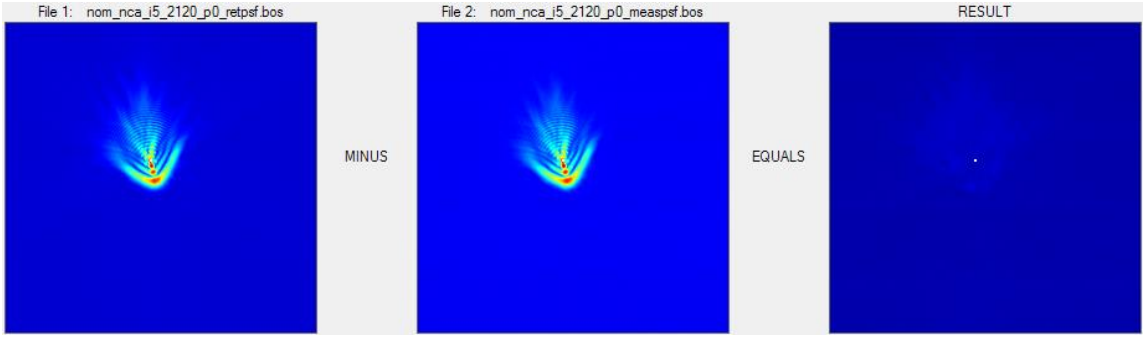

Figure 14. Results of the phase retrieval process on the "I5" source image in NIRCamA at a wavelength of 2120nm. The left image is the amplitude (square root of intensity) of the modeled/retrieved PSF and the middle image is the amplitude of the measured PSF. The difference between the two is shown to the right on the same scale as the modeled and measured images.

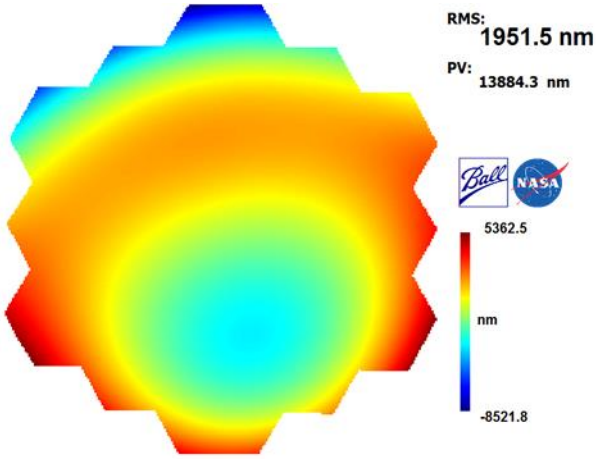

Figure 13. Retrieved wavefront map (tilt removed) over the Fine-Steering Mirror mask for the "I5" source image in NIRCamA at a wavelength of 2120nm.

In addition to the PSF images of the ASPA sources, images of the pupil in the AOS (FSM mask) and the pupil in NIRCamB were collected to examine the relative pupil alignment/shear between the two systems. The relative pupil shear provides additional data on the relative tilt and/or decenter between the AOS and ISIM. The retrieved image and pupil shear parameters are then compared against the model prediction (Figure 16) to produce a measured error vector for each image ([dX_{pixel}, dY_{pixel}, dZ4]) and the pupil ([dX_{Pupil}, dY_{Pupil}]). The measured error vectors for all the images are then passed into a solver to determine the best-fit, rigid-body motion for the ISIM with respect to the AOS that represents the observed errors. The amount of required ISIM rigid body motion is examined along with the residual image location and focus error post ISIM rigid body adjustment

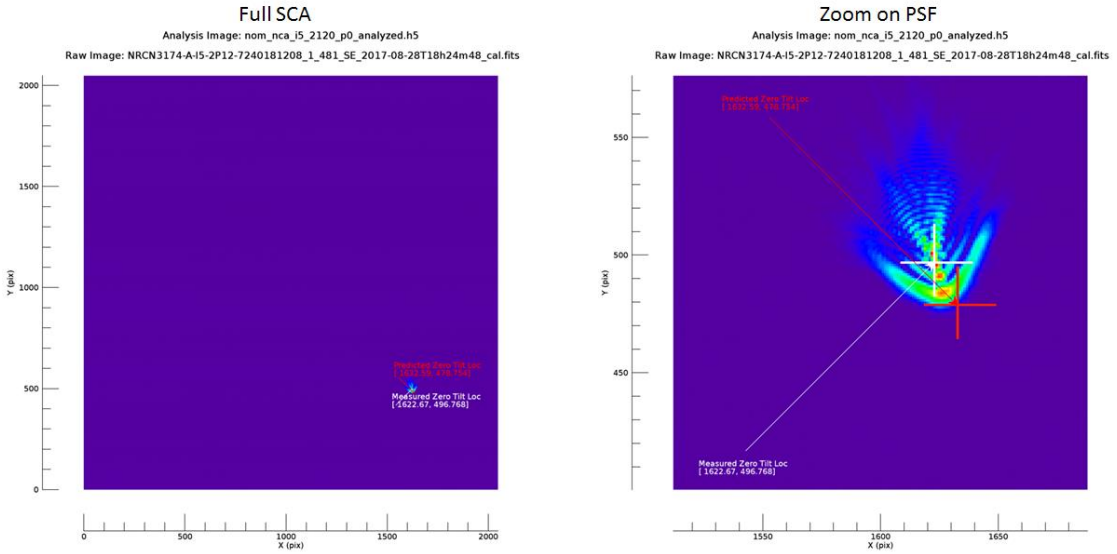

Figure 16. The left image is the full-size sensor chip assembly (SCA) image for the "I5" source in NIRCamA at a wavelength of 2120nm. The right-hand image is a zoom-in on the PSF where the red cross represents the predicted image location and the white cross is the measured image location.

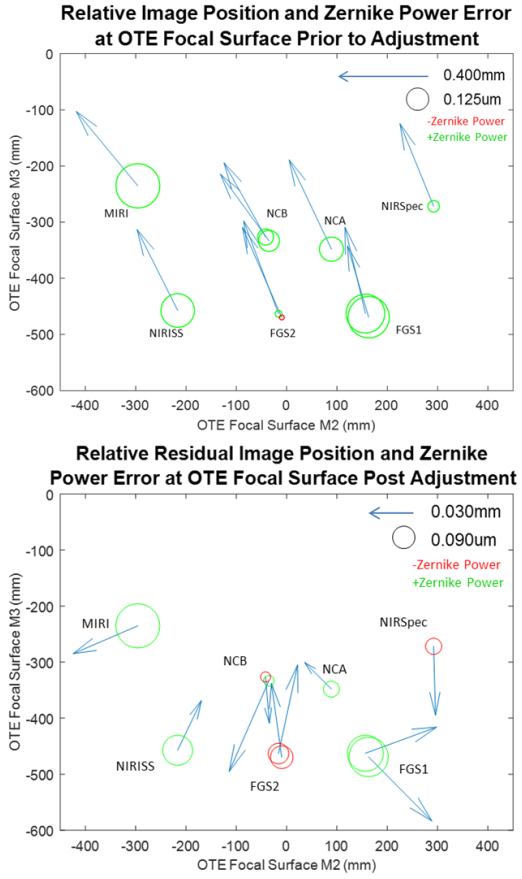

Figure 15. Bubble and vector plots describing the measured image position error (arrows) and Zernike power error (bubbles) over the field of view pre- and post-rigid body adjustment of ISIM.

to evaluate the potential impact to the correctable and uncorrectable degrees of freedom and each individual instruments' focus mechanism.

The correctable degree of freedom for the AOS to ISIM misalignment is focus or motion along the optical axis of AOS and ISIM. This is accommodated by adjusting the axial position of the secondary mirror. For reference, 1mm of AOS to ISIM axial of focus error would require 0.004mm of SM adjustment, which is well within the capability of the ±6mm of on-orbit SM piston motion.

The uncorrectable degrees of freedom for the AOS to ISIM alignment include decenter, tilt, and clocking, all of which primarily affect pupil alignment and ultimately vignetting. Prior to the OTIS cryogenic vacuum test, a set of allowable measured errors between the AOS and ISIM were established based on the prediction/model uncertainty and the metrology uncertainty. These criteria were the action limits that would warrant further investigation if observed differences were larger than the criteria.

The plots in Figure 15 graphically display the measured image position errors and focus/power errors as projected to the OTE focal surface (intermediate image surface between the OTE and ISIM) before and after best-fit ISIM rigid-body motion. It is clear there is a systemic lateral offset to the pre-adjustment image position data

indicating a boresight error. The focus errors as retrieved from phase retrieval indicate individual SI level focus errors vs a systemic focus offset. The best-fit six degree-of-freedom rigid-body motion of the ISIM object surface to the measured data is shown in Table 1 along with the allowable differences based on the prediction and metrology uncertainties ("Yellow Flag Limit"). The table shows that all best-fit rigid body alignment motions are less than the allowable differences indicating an expected alignment.

The residual of the image position errors and focus errors with the best-fit rigid body motion of ISIM removed is graphically shown on the bottom plot of Figure 15 and in Table 2. The residual image position errors are mostly single pixel level or less errors and the residual focus, if real, is within the capture range of each instruments' focus mechanism.

The data and supporting analyses indicate that the Webb Telescope AOS and ISIM are aligned within expectations and have little to no risk for on-orbit operations.

Table 1. Best-fit rigid body motion of ISIM object surface to measured image and pupil errors.

	6DOF	Optical	Yellow Flag Limit
Focus/M1 (mm)	-0.415	-0.415	±1.360
M2 Decenter (mm)	0.207	0.427	±0.605
M3 Decenter (mm)	-0.374		
RM1 Clocking (mrad)	-0.138	-0.138	±1.502
RM2 Tilt (mrad)	0.319	0.322	
RM3 Tilt (mrad)	0.045		

Table 2. Residual image position and focus/power error for each ASPA source image after ISIM object surface rigid body adjustment.

Residual Zero-Tilt Location Error Post ISIM Object Surface Alignment				
ASPA Source	**Instrument**	**dX (pix)**	**dY (pix)**	**dZ4 (um)**
I-1	NCB	0.2	-1.7	-0.019
I-3	NCB	-1.7	-3.4	0.020
I-5	NCA	-1.1	1.0	0.046
I-7	FGS1	-0.5	1.3	0.234
I-9	FGS1	1.1	1.2	0.277
I-11	FGS2	1.5	0.3	-0.076
I-13	FGS2	1.2	-0.2	-0.092
I-15	NIRISS	-0.9	0.5	0.161
I-19	MIRI	0.7	-0.4	0.348
I-25	NIRSpec	-0.6	0.5	-0.047

4.0 SECONDARY MIRROR & PRIMARY MIRROR ALIGNMENT CROSSCHECK RESULTS

The analysis of the data collected during the Pass-and-a-Half (PAAH) test campaign has been completed. An example of the processing that was done on the collected image data of the Hartmann and Inverted Arrays is documented here along with the final assessment of the secondary mirror and primary mirror alignment crosscheck, as well as crosscheck of the relative focus error across the field of view.

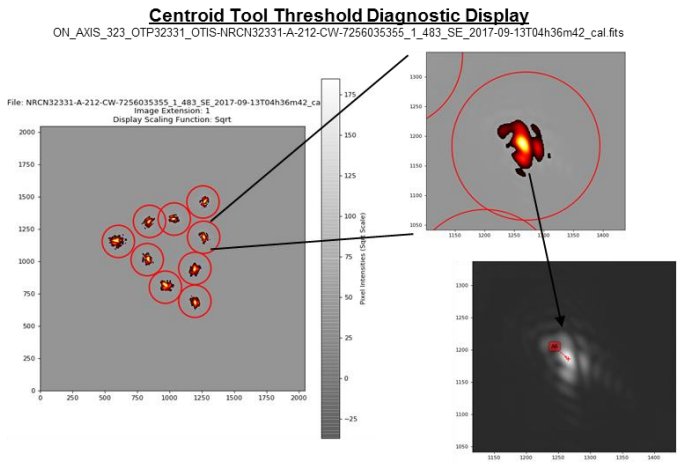

Figure 17. Snapshot of centroiding tool used to process the Hartmann array images.

The image data of the nine Hartmann PSFs was first passed into an analysis tool that quality checked the images, thresholded them, and then centroided the nine unique spots (Figure 17). The located centroids were then passed into another analysis tool that calculated the leg-length differences between the measured and modeled triads (set of A-B-C segments under an ACF). Those differences were then passed into a set of linear equations that were used to solve for the various secondary mirror and primary mirror motions that could fit the observed leg length differences. While simple in processing flow, there is significant nuance in ensuring the model

accurately represents the as-tested configuration in order to produce accurate target PSFs in addition to the nuance in creating the sensitivities for the set of linear equations used in the solver.

Given the subtleties of the solution, a verification test of the sensitivities was devised during the OTIS test to prove that the method and analysis tool was capable of detecting secondary mirror motion. In this test, the Webb secondary mirror was adjusted in position by known amounts with images collected before and after the various adjustments. The data was processed as previously described and the resultant solution compared to the known commanded motion in Table 3. In all degrees of freedom, the analysis tool was able to accurately solve for the observed motion. This provided significant confidence that the tool was able to detect alignment errors as long as the target values provided by the model were correct.

Table 3. Summary of SM adjustment test cases for the Hartmann analysis tool. All commanded degrees of freedom were accurately measured by the analysis process. M1 is the focus axis and M2/M3 are the lateral axes.

SM Influence Pert	*Commanded*			*Measured*			*Error*		
	dM1	dM2	dM3	dM1	dM2	dM3	dM1	dM2	dM3
SM Focus (mm)	0.355	-	-	0.353	-	-	-0.002	-	-
SM Focus (mm)	-0.355	-	-	-0.357	-	-	-0.002	-	-
SM X Tilt (mrad)	-	0.200	-	-0.007	0.193	0.001	-0.007	-0.007	0.001
SM Y Tilt (mrad)	-	-	-0.070	-0.009	-0.011	-0.061	-0.009	-0.011	0.009
SM X Decenter (mm)	-	0.200	-	-0.005	0.204	0.003	-0.005	0.004	0.003
SM Y Decenter (mm)	-	-	-0.100	-0.008	-0.002	-0.096	-0.008	-0.002	0.004

All of the data from the Hartmann Array and the Inverted Array collection was processed and the results are shown in Table 4 along with the corresponding measurement uncertainty and the measurement uncertainty requirement. In all cases except focus, the measured state of the hardware combined with uncertainty is below the uncertainty requirement yielding a ground-aligned system that is well within expectations and requirements. The +0.165mm of SM focus was a known offset left in during test and does not impact the ground-test analysis or conclusions.

Table 4. Summary of the results of the secondary mirror (SM) alignment and relative focus over the field of view. Note that SM tilt and SM decenter are degenerate with each other and the values shown are as is all of the observed error was attributed to one or the other, they are not both present at these levels at the same time.

Degree of Freedom	Measured Value	Measured 2σ Uncertainty	2σ Uncertainty Requirement
SM Focus	+0.165 mm	±0.021 mm	±0.030 mm
SM Tilt (radial)	0.35 mrad	±0.14 mrad	±2.5 mrad
SM Decenter (radial)	0.29 mm	±0.12 mm	±2.1 mm
PM Tilt (radial)	0.036 mrad	±0.015 mrad	N/A
SI Relative Focus (OTE Field Tilt)	1.96 mm (max)	±1.09 mm (max)	±3 mm

As a cross-check to the analysis previously described, another analysis method was applied to the PAAH Hartmann Array and Inverted Array data that used individual PSF measured centroid errors instead of triad leg-lengths to create a wavefront map of the sparse-aperture PAAH pupil. The measured centroid error of each of the nine mirror segments was used to calculate the tilt error over the pie-shaped segment in the pupil. This is what is called the "Reconstructed Sampled Pupil from Hartmann Data" in Figure 18. This approach allows one to fit wavefront perturbations to the reconstructed sampled pupil. In the case of the secondary mirror, wavefront perturbations due to SM focus (power) and SM tilt (coma) can be fit to the reconstructed sampled pupil (this is the "Best-Fit SM Pupil" map in Figure 18). However, in order to perform this fit, the piston and tilt of each ACF must be allowed to vary since that information is not known from the Hartmann test ("Best-Fit Sampled Pupil with ACF Tilt & Piston" below). The optimization metric is the difference between the "Best-Fit Sampled Pupil with ACF Tilt & Piston" and the "Best-Fit SM Pupil" maps as shown to the far right of the figure below.

The table shown in Figure 18 compares the SM rigid-body solution of the Hartmann leg-length approach discussed previously and the wavefront error optimization approach. Both approaches yield the same result to within acceptable levels of the crosscheck. This provides additional confidence in the overall crosscheck of the secondary mirror alignment, primary mirror alignment, and relative focus error across the field.

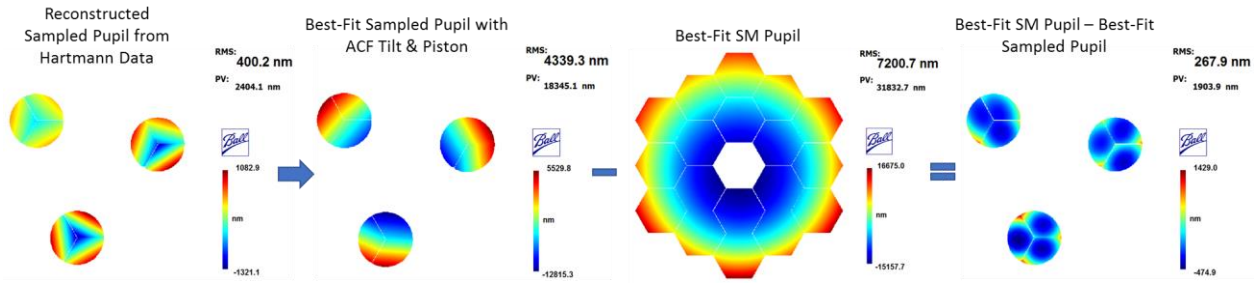

DOF	Hartmann Leg-Length	WFE Optimization
Focus	0.165mm	0.177mm
dRV2	-0.318mrad	-0.309mrad
dRV3	-0.150mrad	-0.035mrad

Figure 18. Sparse-aperture wavefront map reconstruction and best-fit SM perturbation to the reconstructed sparse-aperture map.

The PAAH optical test and corresponding analyses were successful in cross-checking the alignment of the Webb primary mirror and secondary mirror. The purpose of the crosscheck was to verify that the combination of the individual mirror and optical assembly tests combined with target alignment positions supplied by the optical and structural models and then placed into position by photogrammetry would produce optical results that agree with the models. The results described in this section show that the successful cross-check was met well within the pre-test expectations and the allowable on-orbit alignment risks.

5.0 SUMMARY

The results in this paper demonstrate a successful approach used to address the performance risk of a large deployable space telescope mission. The ground testing and verification of large, lightweight, deployable space telescopes is very difficult, and expensive, to achieve with direct verification methods, and will only continue to become more so as telescope sizes increase. Adjusting the scope of the ground testing to prioritize direct verification of the critical few areas (fixed or non-active optical systems, e.g. AOS to ISIM alignment) and then

verifying ground-aligned positions for the active optical systems and ensuring there is adequate adjustment margin to cover model uncertainty and risk (e.g. primary mirror segments and secondary mirror assembly) provides a more reasonable and achievable test approach.

With this test methodology in mind, this paper presented metrology techniques that broke the testing into separable pieces with overlap in order to test the entire system. The first test demonstrated a novel technique to successfully verify alignment of the AOS to ISIM in the presence of significant ground-test wavefront aberration. The second test demonstrated that a sparse-aperture system test of the telescope was successful in verifying the ground-state alignment of the active telescope sub-systems, the primary mirror and secondary mirror, and verify the models used to make those predictions. This testing methodology has successfully managed the risk associated with a large deployable space telescope mission.

6.0 ACKNOWLEDGEMENTS

The James Webb Space Telescope (JWST) project is an international collaboration led by NASA's Goddard Space Flight Center (GSFC) in Greenbelt, MD. Ball Aerospace would like to acknowledge and thank NASA for their leadership, funding, and support during the testing and analysis of the OTIS cryogenic testing campaign. The authors would also like to specifically acknowledge the planning and support from the Webb team at Harris, Inc., the phase retrieval analysis from the Wavefront Analysis team at GSFC, and the analysis support from members of the Space Telescope Science Institute. Finally we would like to thank the many individuals, companies, and government institutions not previously identified who supported the OTIS integration and testing effort at Johnson Space Center.

7.0 REFERENCES

[1] P. A. Lightsey. C. Atkinson, M. Clampin, L. Feinberg, "James Webb Space Telescope: Large Deployable Cryogenic Telescope in Space", Optical Engineering, 51, (2012)

[2] Daniel A. Porpora, Allison A. Barto, Paul A. Lightsey, J. Scott Knight, "Use of living technical budgets to manage risk on the James Webb Space Telescope optical element," Proc. SPIE 9904, Space Telescopes and Instrumentation 2016: Optical, Infrared, and Millimeter Wave, 99043Y (29 July 2016); doi: 10.1117/12.2228620

[3] J. Scott Knight, D. Scott Acton, Paul Lightsey, Adam Contos, Allison Barto, "Observatory alignment of the James Webb Space Telescope," Proc. SPIE 8442, Space Telescopes and Instrumentation 2012: Optical, Infrared, and Millimeter Wave, 84422C (21 September 2012); doi: 10.1117/12.926816

[4] Feinberg, Lee D., "James Webb Space Telescope system cryogenic optical test plans", Proc SPIE 8150 (2011).

[5] Matthews, Gary W., "JWST pathfinder telescope risk reduction cryo test program", Proc SPIE 9575 (2015).

[6] Whitman, Tony, "Non-invasive Optical End-to-End Test of a Large TMA Telescope (JWST) from the Intermediate Focus", SPIE Proc 7438 (2010).

[7] Whitman, Tony, "Measuring the cryogenic optical alignment between the telescope element and the instruments module of the James Webb Space Telescope", SPIE Proc 8146 (2011).

[8] Koby Z. Smith, D. Scott Acton, Ben B. Gallagher, J. Scott Knight, Bruce H. Dean, Alden S. Jurling, Thomas P. Zielinski, "Calibration results using highly aberrated images for aligning the JWST instruments to the telescope," Proc. SPIE 9904, Space Telescopes and Instrumentation 2016: Optical, Infrared, and Millimeter Wave, 990442 (29 July 2016); doi: 10.1117/12.2232180

[9] Knight, J. Scott, "Design of the master optical reference for the James Webb Space Telescope", SPIE Proc 9143 (2014).

[10] Contreras, James, "Nominal Performance and Sensitivity of the James Webb Space Telescope: Optical Telescope Element", SPIE Proc 5487 (2004).

[11] Dean, Bruce H., "Phase Retrieval Algorithm for JWST Flight and Testbed Telescope", SPIE Proc 6265 (2006).

[12] Sharon R. Lunt, David Rhodes, Andrew DiAntonio, John Boland, Conrad Wells, Trevis Gigliotti, Gary Johanning, "Model predictions and observed performance of JWST's cryogenic position metrology system," Proc. SPIE 9904, Space Telescopes and Instrumentation 2016: Optical, Infrared, and Millimeter Wave, 99044C (29 July 2016); doi: 10.1117/12.2231727

[13] James B. Hadaway, Conrad Wells, Gene Olczak, Mark Waldman, Tony Whitman, Joseph Cosentino, Mark Connolly, David Chaney, Randal Telfer, "Performance of the primary mirror center-of-curvature optical metrology system during cryogenic testing of the JWST Pathfinder telescope," Proc. SPIE 9904, Space Telescopes and Instrumentation 2016: Optical, Infrared, and Millimeter Wave, 99044E (29 July 2016); doi: 10.1117/12.2234741

[14] J. Scott Knight, Lee Feinberg, Joseph Howard, D. Scott Acton, Tony L. Whitman, Koby Smith, "Hartmann test for the James Webb Space Telescope," Proc. SPIE 9904, Space Telescopes and Instrumentation 2016: Optical, Infrared, and Millimeter Wave, 99040C (29 July 2016); doi: 10.1117/12.2233114